Aerosol models from the Ocean Color satellite sensors and AERONET-OC, and their impact on reflectance spectra in coastal waters

Eder Herrera[1*], Carlos Carrizo[1], Robert Foster[2] and Alex Gilerson[1]

[1]Optical Remote Sensing Laboratory, the City College of New York, CUNY, New York, NY 10031, USA. [2]Naval Research Laboratory, Washington, DC 20375, USA

ABSTRACT

Atmospheric parameters and remote sensing reflectance from VIIRS and MODIS sensors are compared with counterparts at the eight AERONET sites. Characteristics of aerosols in atmospheric correction models in terms of aerosol optical depth (AOD) were taken from NASA SeaDAS processing software. Significant dependence of AOD differences on the wind speed is demonstrated, which is most likely related to the modeling of the state of the ocean surface in atmospheric correction models and at least partially associated with dependence of sea surface reflectance coefficient on the wavelength, AOD and polarization effects. Analysis of differences in remote sensing reflectance showed dependence on the wind speed and sensor viewing angles, which need to be further studied and corrected.

1. INTRODUCTION

In the field of Ocean Color (OC) the water leaving radiance (Lw) contributes about 10% to the signal measured by a satellite sensor at the top of the atmosphere (TOA). Accurate estimation of the chlorophyll concentration and retrieval of water inherent optical properties (IOP) requires very sophisticated sensor calibration, including so-called system vicarious calibration, and atmospheric correction [1-5]. After eliminating radiance components related to Sun glint[6] and white cap effects[7], the main uncertainty in atmospheric correction is associated with the choice of aerosol models which originally were determined based on data from Shettle and Fenn[8], and then further adjusted based on the data from AErosol RObotic NETwork (AERONET)[9], in current NASA processing. In the open ocean, the black pixel approximation is applicable[10] where the signal from water at the NIR bands near 748 and 865nm is assumed negligible. In coastal areas with stronger backscattering from water, additional iterations are required for the NIR algorithms[4] or a NIR-SWIR approach is applied[11] for waters with high turbidity. Nevertheless, in coastal areas, satellite-derived remote sensing reflectance in the blue bands (410, 443nm) is often less accurate than in the green and red bands and the uncertainties are usually associated with the aerosol models used in the atmospheric correction.

Validation of the chosen aerosol models is difficult and the most viable option is the comparison of the aerosol parameters with the ones measured by AERONET for Ocean Color (AERONET-OC) SeaPRISM instruments. This AERONET-OC network[12] which was noticeably expanded in the US and globally in the last few years has the instruments installed on the ocean platforms and provides data on both aerosol parameters and remote sensing reflectance, R_{rs}, from the surrounding water body.

*eherrer002@citymail.cuny.edu

Aerosol models are characterized by the particle size distribution, by the fractions of coarse and fine aerosol modes, the concentration of particles, their refractive indices, shape, and relative humidity. These are then transformed into phase functions (PF) which characterize a probability of light scattered in different directions, aerosol optical depth (AOD), which determines the amount of aerosols in the atmospheric layer and a single scattering albedo which takes into account absorbing effects.

In our recent paper[13], we analyzed data of AOD and phase functions for two sites: on Long Island Sound Coastal Observatory (LISCO) and WaveCIS in the Gulf of Mexico and for the Visible-Infrared Imager Radiometer Suite (VIIRS) satellite sensor showing that for both sites PF functions measured at AERONET stations in about 90% of the cases do not lay between minimum and maximum PF expected from the atmospheric correction model and that the relative difference between satellite and AERONET AOD depends on the wind speed. The latter was associated with the satellite processing of the ocean surface effects and at least partially with the reflectance coefficient ρ of skylight from the ocean surface. This issue was discussed in details in Gilerson et al[14] demonstrating strong impact of AOD and PF on ρ in various observational and surface conditions and through it on the retrieval of the water leaving radiance and R_{rs} from above water and satellite observations.

In this paper, we expand our comparisons between satellite and AERONET-OC data to both VIIRS and the Moderate Resolution Imaging Spectroradiometer (MODIS) sensors, and to eight AERONET-OC sites. Analysis is further expanded to NOAA MSL12 processing of VIIRS data.

2. BACKGROUND

In ocean color satellite data processing, the atmospheric correction procedure, which eliminates the perturbing effects of the atmosphere and ocean surface, is the most important step. Notably, the Near Infrared (NIR) algorithm developed by Gordon and Wang[3] which makes use of near-infrared bands in initial estimations of water-leaving radiance with further improvements and expansions to the Short Wave Infrared (SWIR) algorithm and combined approach[15] have been successfully used in the processing of ocean color (OC) data.

Total radiance measured from a space-borne OC sensor at a wavelength (λ), denoted as $L_t(\lambda)$, can be described as following neglecting white caps effects as a first approximation[2, 16]:

$$L_t(\lambda) = L_r(\lambda) + L_a(\lambda) + L_{ra}(\lambda) + T_s(\lambda)L_g(\lambda) + t(\lambda)L_w(\lambda) \qquad (1)$$

L_r and L_a are the radiances resulting from multiple scattering by air molecules (Rayleigh scattering) and aerosols, respectively. L_{ra} is the interaction term between molecular and aerosol scattering[2, 17], L_g is the radiance of the direct solar beam, L_w is the water-leaving radiance. T_s and t are the direct and the total atmospheric transmittance from surface to sensor direction respectively. Eq. (1) is also often represented in terms of reflectance values where radiances are multiplied by $\pi / F_0 \cos\theta_0$, where F_0 is the extraterrestrial solar irradiance[18], and θ_0 is the solar zenith angle.

The L_g term is generally parameterized based on the wind speed for a given viewing geometry[6] using the Cox and Munk model[19]. Similarly, L_r can be also well predicted from the atmospheric pressure and wind speed [10, 20, 21]. After removing Rayleigh and Sun glint components Eq. (1) is modified as

$$L_t(\lambda) = \underbrace{L_a(\lambda) + L_{ra}(\lambda)}_{L_A} + t(\lambda)L_w(\lambda) \quad (2)$$

The aerosol component $L_A(\lambda)$ is estimated through the NIR atmospheric correction algorithm [2] by the calculation of the ratios (epsilon) of reflectances at two NIR bands. This is currently implemented with the set of 80 aerosol models defined by Ahmad et al [9]. L_a is calculated as [2]

$$L_a(\lambda) = \frac{\omega_a(\lambda)\tau_a(\lambda)p_a(\theta_0,\theta_v,\lambda)}{4\cos\theta_v\cos\theta_0}\frac{F_0\cos\theta_0}{\pi} \quad (3)$$

where $\omega_a(\lambda)$ is the single scattering albedo, $\tau_a(\lambda)$ is the aerosol optical depth (AOD), $p_a(\theta_v,\theta_0,\lambda)$ is the aerosol phase function (PF) which also takes into account reflectance from the surface, θ_v is the sensor zenith angle. The iterative nature of the atmospheric correction process in coastal waters means that $\tau_a(\lambda)$ and $p_a(\theta_v,\theta_0,\lambda)$ values determine, and in turn are determined by the selected models, which might mean that they depend on the accuracy of the model selection. In addition, τ_a is included directly in the aerosol reflectance component as in Eq. (3) and in the exponential terms of T_s and t and is determined in the atmospheric correction process in several (usually two) approximations[4]. At the same time, it should be noticed that inaccuracies in calculations of some of the components in Eq (1) can be artificially "compensated" by the changes in AOD.

The standardized parameters based on retrieved L_w, normalized water-leaving radiance $nLw(\lambda)$ and remote sensing reflectance $R_{rs}(\lambda)$ are calculated as

$$nLw(\lambda) = D^2\frac{L_w(\lambda,\theta_0,\theta_v,\varphi)}{\cos\theta_0 t_d(\lambda)} \quad (4)$$

$$R_{rs}(\lambda) = nLw(\lambda) \,/\, F_0(\lambda) \quad (5)$$

or

$$R_{rs}(\lambda) = Lw(\lambda) \,/\, E_d(\lambda) \quad (5a)$$

where φ is the azimuth angle, t_d is the diffuse atmospheric transmittance along the Sun-to-surface direction, D^2 is the Sun-Earth distance in astronomical units, and $E_d(\lambda)$ is the downwelling irradiance near the surface. Eq. (4) needs to be corrected for the bidirectional reflectance distribution function (BRDF) which is the correction factor for illumination and viewing geometries dependency and which is the function of the water constituents [22-26].

In our analysis of AOD and Rrs, we define ΔAOD and ΔRrs as the relative error between AERONET and sensor (VIIRS or MODIS) values:

$$\Delta AOD = \frac{AOD(\lambda)_{sensor} - AOD(\lambda)_{AERONET}}{AOD(\lambda)_{AERONET}} \quad (6)$$

$$\Delta R_{rs} = \frac{R_{rs}(\lambda)_{sensor} - R_{rs}(\lambda)_{AERONET}}{R_{rs}(\lambda)_{AERONET}} \quad (7)$$

3. APPROACH

3.1 Satellite data filtering procedures

The VIIRS and MODIS Level 2 images processed with the SeaDAS software package using standard iterative NIR atmospheric correction algorithm[10, 27, 28] have been obtained for the regions over eight sites at the Northern Hemisphere, the Long Island Sound Coastal Observatory (LISCO), WaveCIS, COVE, MVCO, USC SeaPRISM, Gloria, Helsinki Lighthouse, and Venice, for the period of January 2012 to December 2016 from NASA OBPG website (https://oceancolor.gsfc.nasa.gov). All VIIRS and MODIS-Aqua data used are from the most recent processing version, 2018.0. In addition, VIIRS data were used with the NOAA MSL12 data processing for the same period of time and were obtained from NOAA Coast Watch website (ftp://ftp.star.nesdis.noaa.gov/pub/socd1/mecb/coastwatch/viirs/science/L2/) with the most recent processing version, SCI_OC04.0_V1.20.

These standard Level 2 data files include the geophysical products of the atmospheric-ocean system, namely the aerosol optical depth (τ_a), the remote sensing reflectance (R_{rs}) and the level 2 quality flags. The VIIRS and MODIS data used in this study are with nadir resolutions of 750 m and 1 km respectively. The pixels used for matchup comparison are all extracted from a region (3x3 pixel box) centered at the site locations. In this study, we utilized the standard scheme, in which spatial average of satellite data from the region of interest is evaluated against in-situ data[19]. In this approach, data affected by unexpected changes in the natural and environmental conditions as well as artifacts in the satellite image resulting from the sensor's intrinsic characteristics are excluded from the analysis. This is done by excluding pixels that have been flagged, through the data processing, by at least one of these conditions: land, cloud, failure in atmospheric correction, stray light (except for LISCO), bad navigation quality, both high and moderate glint, negative Rayleigh-corrected radiance, viewing angle larger than 60°, and solar zenith angle larger than 70°. Moreover, any individual pixel which has water-leaving radiance spectrum with negative values in any wavelength is also excluded from spatial averaging. For the R_{rs} comparisons analysis is carried out in reference to the SeaPRISM wavelengths (413, 442, 491, 551, and 668 nm) even though the satellite sensor wavelengths are slightly different from those of SeaPRISM for some channels. For AOD comparisons, bands 443, 667 and 870 nm are used.

3.2 In- situ AERONET-OC data

The ocean color component of the Aerosol Robotic Network (AERONET – OC) [12] has been implemented to support long-term satellite ocean color investigations. This is done through consistent and accurate cross-site measurements collected by the SeaPRISM autonomous radiometer systems, deployed on offshore fixed platforms. In addition to these ocean color measurements, the regular data acquisitions of AERONET are also carried out, which permit accurate retrievals of the AOD and the fine-coarse aerosol mode fraction. The SeaPRISM level 1.5 data are used in this study as in-situ OC data to evaluate the VIIRS and MODIS data.

At the LISCO platform[29] the instrument is positioned on a retractable tower with an elevation of 12 m. It was installed in October 2009 and has been providing data since then. Periodic recalibration of the LISCO SeaPRISM instrument by NASA (most recent in March 2017) showed 0-1% deviations/year for all bands. The WaveCIS site is located at approximately 18 km

from the shore of Timbalier Bay area, MS, USA. Brief information about all AERONET-OC sites studied is given in Table 1.

All in-situ data used in the quantitative match up comparison analysis are selected and averaged from the measurements made within a ±2 hour time window of the satellite overpass time of the locations of the sites for R_{rs}, and within ±10 min time window for AOD. This approach ensures that the in-situ data set that is minimally affected by the natural temporal changes in the atmosphere and water and it is also in line with the similar validation exercises carried out for other OC sensors[12].

4. RESULTS AND DISCUSSION

VIIRS' Remote sensing reflectance for five bands separately and all combined for both LISCO, and WaveCIS sites compared with AERONET data is shown in Fig. 1 for 2012-2016. Both stations demonstrate vulnerability to atmospheric correction for the blue band at the WaveCIS site and all bands, especially blue, for more coastal LISCO site. Results are similar for the MODIS sensor. Corresponding AOD matchups which include both VIIRS and MODIS data are shown in Fig. 2 with a strong overestimation of AOD on both sensors for the LISCO site and smaller but measurable overestimation for WaveCIS, thus encouraging a deeper analysis of the AOD retrievals. MODIS bias is smaller than VIIRS bias on the retrieval of AOD for both LISCO and WaveCIS sites but overall both sensors give similar results.

One of the most important findings[13] was the dependence of ΔAOD on the wind speed. This result is confirmed here by data from all eight AERONET sites and both satellite sensors in Fig. 3 which shows a clear dependence of ΔAOD (869) on the wind speed. VIIRS ΔAOD has a steeper slope (m=0.3) than MODIS ΔAOD (m=0.2). The spread of data unexpectedly decreases with wind speed, W, till $W \approx 4 - 5m/s$. This wind speed dependence, which should not exist in ideal processing, was attributed [13] to the state of the ocean surface which is supposed to have a small impact on the AERONET data (through the correction for the underlying surface in the retrieval algorithm) but is included in the Sun glint correction algorithm[6] and in the modeling of the Rayleigh reflectance component[15] which includes reflectance coefficient ρ from the ocean surface[30-32].

Variability of ρ for various wind conditions and aerosol loads were further studied by us[14]. Zhang et al[32] has also shown that unavoidable Sun glint can have a noticeable impact on ρ for high Sun positions and viewing angles ≤40°. Results of simulations[10] using vector radiative transfer code (VRT)[33] demonstrated the significant variability of ρ on the wavelength, wind speed and viewing angle. The inaccuracies in the atmospheric correction procedures which do not fully account for the variability of ρ affect near surface and TOA radiances and can have an impact on the above water measurements, AERONET-OC and satellite data. The retrieval of the water leaving radiance from satellite data can be affected by the corresponding errors in the calibration and atmospheric correction processes[14]. Some of the effects in TOA radiances can be partially compensated by the non-optimal choice of aerosol models. This will result in the PF functions falling outside prescribed min-max brackets and inaccurate AOD retrievals described above[13].

Further, several comparisons of R_{rs} from AERONET-OC and satellite data were carried out as they can be affected by uncompensated inaccuracies in processing from both sides. Fig. 4a-d

shows that ΔRrs averaged for all sites is increasing with wind speed for both VIIRS and MODIS. In VIIRS MSL12 processing (Fig. 4e-f) ΔRrs is slightly higher than in NASA processing but the trend is the same. Preliminary analysis shows that the ΔRrs wind speed dependence can be associated with the inaccuracies of AERONET-OC algorithm for total radiance but this and other possible reasons of dependence should be further studied and corrected to ensure better matchup of satellite and AERONET-OC data.

Because of dependence of the ρ coefficient on the viewing angle ΔRrs was analyzed as a function of the sensor-viewing angle with results for 410 nm are shown in Fig. 5a, c. For 443nm there is a clear trend (and it is the same for all other wavelengths) of ΔRrs decrease about 10% with the viewing angle (Fig. 5b, d). These differences are fully due to the satellite processing algorithms and should be further studied. In addition, for 410 nm there is a strong increase of the standard deviation for ΔRrs at the sensor viewing angles near 20°, which obviously contributes to the overall uncertainties typical for 410 nm. This effect can be preliminary attributed to the difficulties in Sun glint correction but should be further analyzed as a function of wind speed and Sun zenith angle.

5. CONCLUSIONS

Data for aerosol parameters, primarily aerosol optical depth (AOD), used in the atmospheric correction models for the VIIRS and MODIS imageries are compared with the data from eight AERONET – Ocean Color (OC) stations in the US and Europe.

VIIRS and MODIS AOD values exceed AERONET-OC AOD values almost at all matching measurements. Previously determined dependence of ΔAOD on the wind speed is confirmed for both satellites and on the average for all studied AERONET-OC stations. This effect is attributed at least partially to the dependence of surface reflectance coefficient on the AOD and is analyzed together with recent results[14].

Analysis of ΔRrs trend as function of wind speed reveals difference, which are most likely to be corrected by improved AERONET-OC data processing of above water radiances. Dependence of ΔRrs on the viewing angle and significant increase of the standard deviation for ΔRrs around 20° at 410nm require further attention and more detailed studies.

ACKNOWLEDGEMENTS

We acknowledge NOAA CREST, JPSS Cal/Val and NASA OBB programs for the support of this work, NASA Ocean Color Processing Group for the satellite imagery and SeaDAS software, NASA AERONET group and PIs for AERONET-OC sites for data on aerosols and remote sensing reflectance.

REFERENCES

[1] Franz, B.A., Bailey, S.W., Werdell, P.J., McClain, C.R., "Sensor-independent approach to the vicarious calibration of satellite ocean color radiometry," Applied Optics, 46, 5068-5082 (2007).

[2] Gordon, H.R., Wang, M., "Retrieval of water leaving radiance and aerosol optical thickness over the oceans with SeaWiFS: a preliminary algorithm," Applied Optics, 33, 443-458 (1994).

[3] Gordon, H.R., "In-orbit calibration strategy for ocean color sensors," Remote Sensing of Environment, 63, 265-278, (1998).

[4] Mobley, C., Werdell, J., Franz, B., Ahmad, Z., Bailey, S., "Atmospheric Correction for Satellite Ocean Color Radiometry," NASA/TM–2016-217551 (2016).

[5] Wang, M., Shi, W., Jiang, L., Voss, K., "NIR- and SWIR-based on-orbit vicarious calibrations for satellite ocean color sensors," Optics Express, 24, 20437-20453 (2016).

[6] Wang, M., Bailey, S.W., "Correction of sun glint contamination on the SeaWiFS ocean and atmosphere products," Applied Optics, 40, 4790-4798 (2001).

[7] Frouin, R., Schwindling, M., Deschamps, P.Y., "Spectral reflectance of sea foam in the visible and near-infrared: In situ measurements and remote sensing implications," Journal of Geophysical Research, 101, 14361-14314 (1996).

[8] Shettle, E.P., Fenn, R.W., "Models for the aerosols of the lower atmosphere and the effects of humidity variation on their optical properties," Environ. Res. Paper 676, AFGL-TR-79-0214.1979 (1979).

[9] Ahmad, Z., Franz, B.A., McClain, C.R., Kwiatkowska, E.J., Werdell, J., Shettle, E.P., Holben, B.N., "New aerosol models for the retrieval of aerosol optical thickness and normalized water-leaving radiances from the SeaWiFS and MODIS sensors over coastal regions and open oceans," Applied Optics, 49, 5545-5560 (2010).

[10] Siegel, D.A., Wang, M., Maritorena, S., Robinson, W., "Atmospheric correction of satellite ocean color imagery: the black pixel assumption," Applied Optics, 39, 3582-3591 (2000).

[11] Wang, M., "A refinement for the Rayleigh radiance computation with variation of the atmospheric pressure," International Journal of Remote Sensing, 26, 5651–5663 (2005).

[12] Zibordi, G., Mélin, F., Berthon, J.F., Holben, B., Slutsker, I., Giles, D., D'Alimonte, D., Vandemark, D., Feng, H., Schuster, G., "AERONET-OC: a network for the validation of ocean color primary products," Journal of Atmospheric and Oceanic Technology, 26, 1634-1651 (2009).

[13] Gilerson, A., E. Herrera, Y. Klein, R. Foster, B. Gross, R. Arnone, S. Ahmed, "Characterization of aerosol parameters over ocean from the Ocean Color satellite sensors and AERONET-OC data," Proc. of SPIE 10422, Warsaw, Poland, Sept. 2017.

[14] Gilerson, A., C. Carrizo, R. Foster, T. Harmel, "Variability of the reflectance coefficient of skylight from the ocean surface and its implications to Ocean Color, " Optics Express, 26, 9615-9633, 2018.

[15] Wang, M.H., Shi, W., "The NIR-SWIR combined atmospheric correction approach for MODIS ocean color data processing," Optics Express, 15, 15722-15733 (2007).

[16] IOCCG, "Atmospheric Correction for Remotely-Sensed Ocean-Colour Products," Wang, M. (Ed.), Reports of International Ocean-Color Coordinating Group, No. 10, IOCCG, Dartmouth, Canada (2010).

[17] Deschamps, P.Y., Herman, M., Tanre, D., “Modeling of the atmospheric effects and its application to the remote sensing of ocean color,” Applied Optics, 22, 3751-3758 (1983).
[18] Thuillier, G., Herse, M., Labs, D., Foujols, T., Peetermans, W., Gillotay, D., Simon, P.C., Mandel, H., “The solar spectral irradiance from 200 to 2400 nm as measured by the SOLSPEC spectrometer from the ATLAS and EURECA missions,” Solar Physics, 214, 1-22 (2003).
[19] Cox, C., Munk, W., “Statistics of the sea surface derived from sun glitter,” Journal of Marine Research, 13, 198-227 (1954).
[20] Gordon, H. R., Wang, M., “Surface roughness considerations for atmospheric correction of ocean color sensors. 1: The Rayleigh scattering component,” Applied Optics, 31, 4247–4260 (1992).
[21] Wang, M., “The Rayleigh lookup tables for the SeaWiFS data processing: Accounting for the effects of ocean surface roughness,” International Journal of Remote Sensing, 23, 2693–2702 (2002).
[22] Gordon, H.R., “Normalized water-leaving radiance: revisiting the influence of surface roughness,” Applied Optics, 44, 241-248 (2005).
[23] Hlaing, S., Gilerson, A., Harmel, T., Tonizzo, A., Weidemann, A., Arnone, R., Ahmed, S., “Assessment of a bidirectional reflectance distribution correction of above-water and satellite water-leaving radiance in coastal waters,” Applied Optics, 51, 220-237 (2012).
[24] Morel, A., Antoine, D., Gentili, B., “Bidirectional reflectance of oceanic waters: accounting for Raman emission and varying particle scattering phase function,” Applied Optics, 41, 6289-6306 (2002).
[25] Voss, K.J., Morel, A., “Bidirectional reflectance function for oceanic waters with varying chlorophyll concentrations: Measurements versus predictions,” Limnology and oceanography, 698-705 (2005).
[26] Wang, M., “Effects of ocean surface reflectance variation with solar elevation on normalized water-leaving radiance,” Applied Optics, 45, 4122-4128 (2006).
[27] Bailey, S.W., Franz, B.A., Werdell, P.J., “Estimation of near-infrared water-leaving reflectance for satellite ocean color data processing. Optics Express, 18, 7521-7527 (2010).
[28] Bricaud, A., Morel, A., Babin, M., Allali, K., Claustre, H., “Variations of light absorption by suspended particles with chlorophyll a concentration in oceanic (case 1) waters: analysis and implications for bio-optical models,” Journal of Geophysical Research, 103, 31033-31044 (1998).
[29] Harmel, T., Gilerson, A., Hlaing, S., Tonizzo, A., Legbandt, T., Weidemann, A., Arnone, R., Ahmed, S., “Long Island Sound Coastal Observatory: assessment of above-water radiometric measurement uncertainties using collocated multi and hyperspectral systems,” Applied Optics, 50, 5842-5860 (2011).
[30] Foster, R., Gilerson, A. “Polarized transfer functions of the ocean surface for above-surface determination of the vector submarine light field,” Applied Optics, 55, 9476-9494 (2016).
[31] Mobley, C., “Estimation of the remote-sensing reflectance from above-surface measurements,” Applied Optics, 38, 7442-7455 (1999)
[32] Mobley, C., “Polarized reflectance and transmittance properties of windblown sea surfaces,” Applied Optics, 54, 4828-4849 (2015).
[33] Zhang, X., S. He, A. Shabani, P.W. Zhai, K. Du, "Spectral sea surface reflectance of skylight,” Opt. Exp. 25(4), A1-A13 (2017).

TABLES AND FIGURES

Table 1. Location and parameters of AERONET-OC sites.

Station name	Location	Distance to shore (km)	Latitude (°)	Longitude (°)	Height above water (m)
LISCO	Long Island Sound near Northport, NY, USA	3.00	N 40.955	W 73.342	12.0
WaveCIS Site CSI 6	Timbalier Bay area, MS, USA	18.00	N 28.867	W 90.483	32.7
MVCO	Near South Beach in Edgartown, MA, USA	5.00	N 41.300	W 70.550	10.0
COVE SeaPRISM	Near Virginia Beach, VA, USA	25.00	N 36.900	W 75.710	24.0
USC SeaPRISM	Near Newport Beach, CA, USA	18.00	N 33.564	W 118.118	31.0
Helsinki Lighthouse	Gulf of Finland	27.78	N 59.949	E 24.926	20.0
Gloria	Near Constanta, Romania	22.22	N 44.599	E 29.360	30.0
Venice	Venice Lagoon, Italy	14.82	N 45.314	E 12.508	10.0

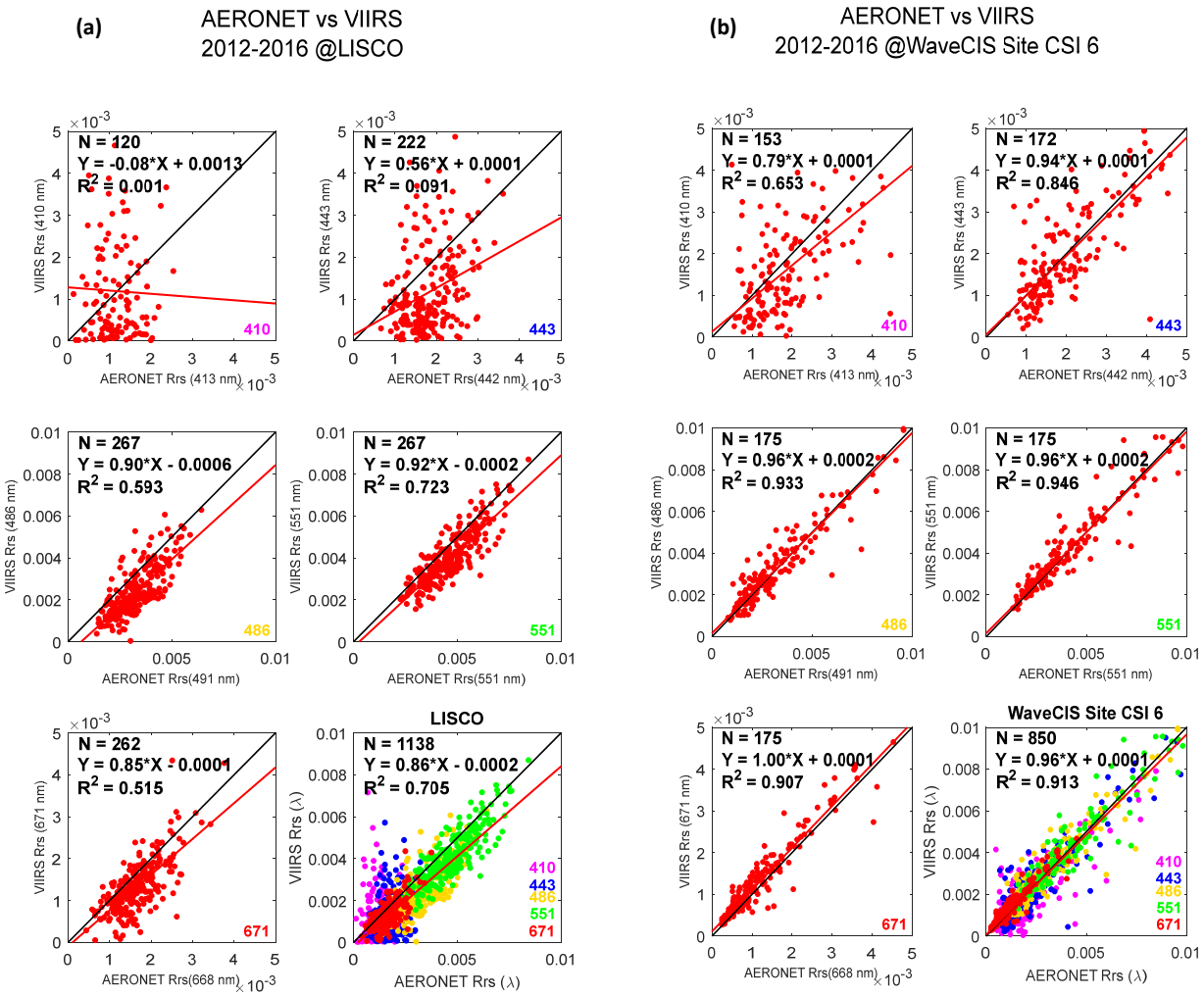

Figure 1. R_{rs} for VIIRS sensor, (a) LISCO site and (b) WaveCIS site, at five wavelengths and all combined, for period 2012-2016.

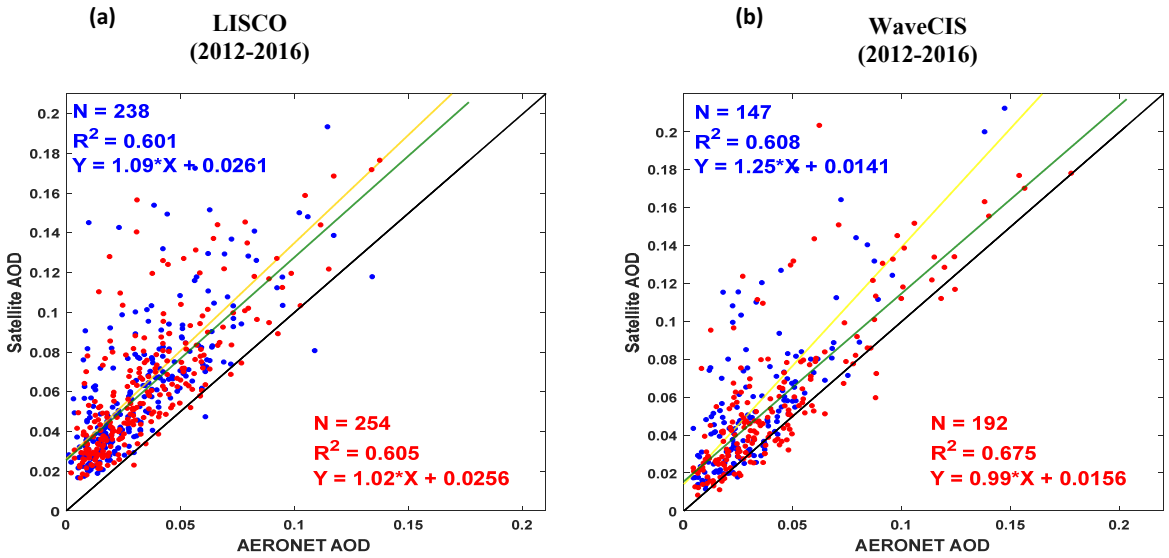

Figure 2. AOD matchups for LISCO (a) and WaveCIS (b) sites. VIIRS (blue dots and yellow regression line), and MODIS (red dots and green regression line) sensors overestimate AOD values compared to AERONET-OC. Both sensors have similar correlation values.

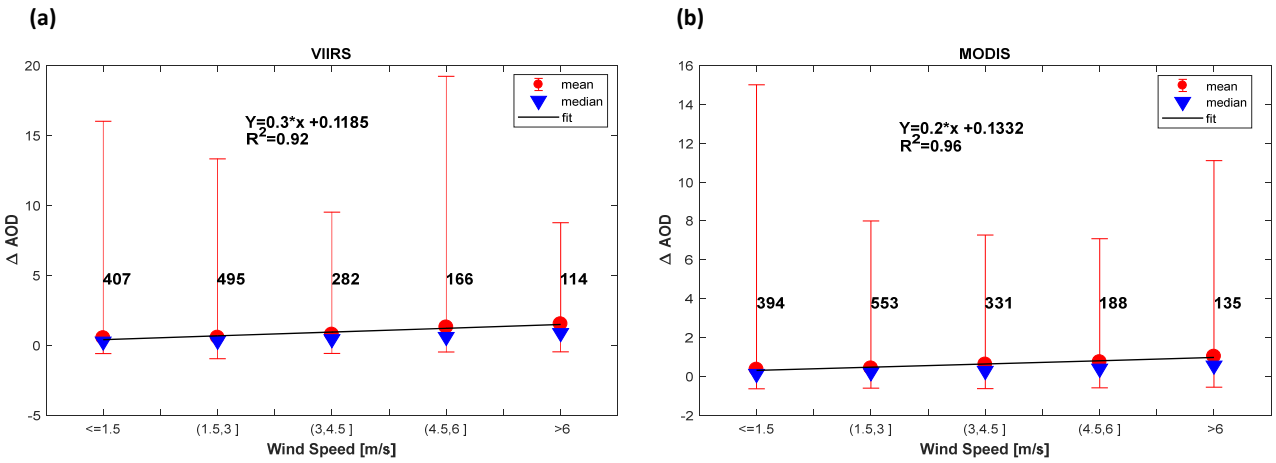

Figure 3. Dependence of ΔAOD for VIIRS (a) and MODIS (b) sensors (NASA processing) as a function wind speed (m/s). Red bars show the full range of ΔAOD at the specified wind speed range.

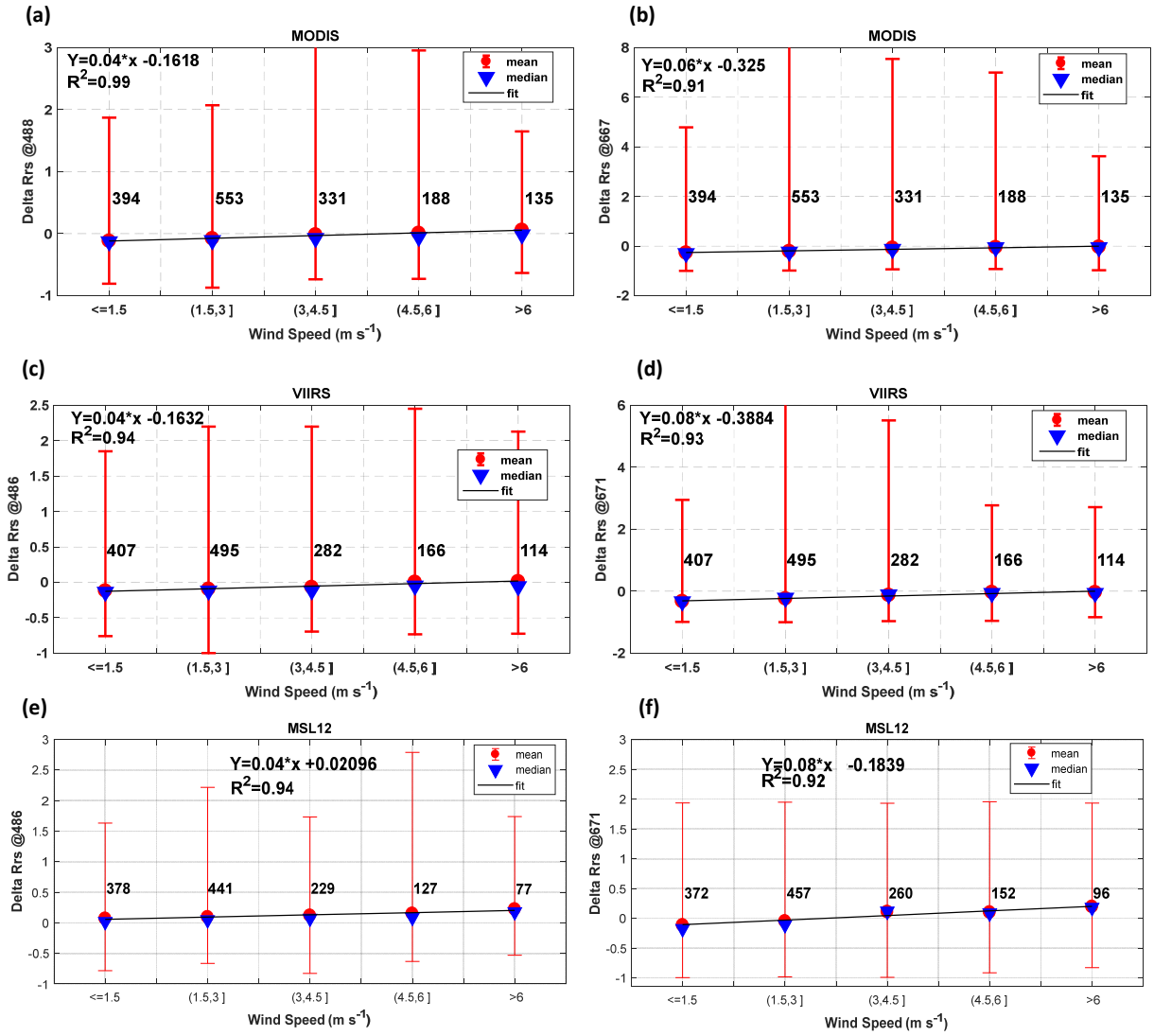

Figure 4. Dependence of ΔRrs on the wind speed (m/s) at wavelengths 488 nm (a) and 667 nm (b) for MODIS, and wavelength 486 nm (c) [e] and 671 nm (d) [f] for VIIRS (NASA processing) and [MSL12] (NOAA processing). Red bars show the full range of ΔRrs at the specified wind speed range.

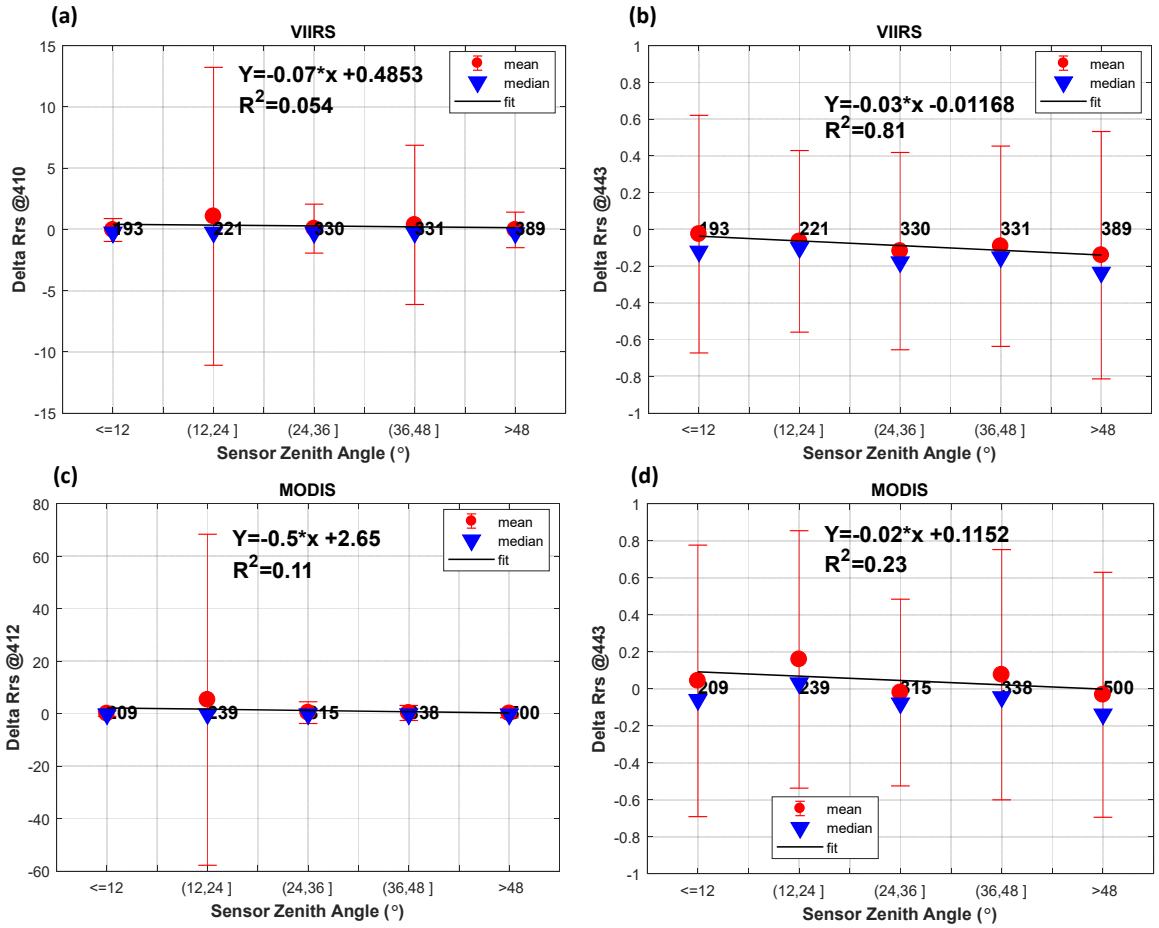

Figure 5. ΔRrs for 410 [443] nm as a function of the sensor-viewing angle, which has angles bigger than zero degree and lower than sixty degrees, for VIIRS (a)[b] and MODIS (c)[d] (NASA processing). Red bars show a standard deviation of ΔRrs at the specified sensor zenith angle's range.